Spatiotemporal Characterization of of the impact of Hurricane Michael on Urban Vegetation Cover in Panama City and Panama City Beach, Florida

Asiful Alam (sa15452@uga.edu)
University of Georgia Warnell School of Forestry and Natural Resources https://orcid.org/0000-0001-9024-1681

Deepak R. Mishra
University of Georgia Department of Geography

Puneet Dwivedi
University of Georgia Warnell School of Forestry and Natural Resources

Research Article

Keywords: Land Cover, Normalized Difference Water Index, Enhanced Vegetation Index, Census County Divisions, Optimized Hotspot and Outlier Analysis

Posted Date: September 7th, 2022

DOI: https://doi.org/10.21203/rs.3.rs-2019241/v1

Abstract

The impacts of major climatic events on urban vegetation cover are not well understood. We used Landsat 8 ETM + derived land cover in Google Earth Engine (GEE) to determine damage to urban vegetation, and Optimized Hotspot and Outlier Analyses to identify significant spatial clusters of hotspots and cold spots from Hurricane Michael in Panama City and Panama City Beach, Florida. We used two vegetation indices (Normalized Difference Water Index-NDWI and Enhanced Vegetation Index-EVI) to assess the impact of Hurricane Michael on urban vegetation cover. Results show that more than 30.07% of the land cover changed after two months of the hurricane landfall, including a rapid increase of 19.64% in water bodies. Overall, we observed a 4.91% decrease in vegetation cover, out of which 34.44% were coastal woody wetlands. NDWI showed a rapid increase due to an increase in water coverage in the study area, whereas EVI decreased due to vegetation loss by strong winds and intense precipitation. After Hurricane Michael, hotspots for high water content in sustained vegetation (NDWI) and overall vegetation condition (EVI) were discovered in Panama City Beach, Southport, and Youngstown CCD (census county division). Statistically significant (≥ 95% confidence, $z \geq 1.96$) increases in NDWI hotspots (76.11% of the total area) were observed post-hurricane due to an increase in water bodies. EVI showed a decrease of about 9.21% in hotspot areas (≥ 95% confidence, $z \geq 1.96$) due to defoliation caused by hurricane force winds. Our results highlight the advantages of using spatial statistical methods that could aid the development of natural hazard mitigation plans and risk reduction strategies by characterizing urban vegetation status in the Gulf Coast from previous hurricane occurrences spatiotemporally.

1. Introduction

Hurricanes are major natural threats to the Gulf Coast states (The Atlantic 2017). In their 2022 Atlantic Hurricane Season Outlook, the National Hurricane Center (NHC) anticipates a likely range of 14 to 21 storms, of which 6 to 10 could develop into hurricanes (winds of 74 mph or higher), including 3 to 6 significant hurricanes (category 3, 4 or 5; with winds of 111 mph or higher) (NOAA 2022). The total approximate cost of damages from tropical cyclones and hurricanes on the Gulf Coast from 1980 to 2020 has been about $790 billion (NOAA 2021a; NCEI 2022). In addition to the economic loss, hurricanes take several lives every year. Hurricanes have claimed about 3,163 lives since 1980, and the devastating hurricane Katrina alone in 2005 left more than 2,000 people dead along the Gulf Coast (Fig. 1).

In addition to devastating casualties and financial losses, hurricanes also seriously harm the coastal ecology, changing the land cover (NOAA 2018, 2020, 2021b). For example, about 320 million large trees were severely damaged by Hurricane Katrina (Chambers et al. 2007; NASA 2007), and Hurricane Laura destroyed 900,000 acres of forested land along the Gulf Coast, resulting in an overall $63 million in economic loss (USDA 2020). Hurricane Ike (2008) resulted in the removal of 4.3% of all trees measured in Houston, Texas. Approximately 1,000 square miles of coastal woody wetland were lost or changed to other land cover types between 1996 and 2010 due to catastrophic hurricanes and tropical cyclones on the Gulf Coast (NOAA 2018). Louisiana alone lost more than 160 square miles of wetland area to water after Hurricane Katrina (NOAA 2005, 2021b).

Some studies have quantified the effects of hurricanes on forest ecosystems using advanced geospatial techniques. Ramsey et al. (1997) used AVHRR 250m multi-temporal images to analyze the effects of 1992 Hurricane Andrew on forests. They found that regional averaged NDVI (Normalized Difference Vegetation Index) change followed damage severity but did not provide a quantitative relationship between NDVI change and damage severity. Ayala-Silva and Twumasi (2004) used the standardized change of NDVI produced from AVHRR data to assess forest damage brought on by Hurricane Georges in 1998. They inferred the linear relationship between regional averaged NDVI and the length of the hurricane track. Using local scale data from the Advanced Spaceborne Thermal Emission and Reflection Radiometer (ASTER) satellite, Aosier et al. (2007) investigated the effects of 2004 Typhoon Songda on vegetation cover. They discovered that the change in adjusted NDII (Normalized Difference Infrared Index) was smaller than the change in NDVI (Normalized Difference Vegetation Index) for damaged trees. Their results were at odds with earlier research, which found that NIR-SWIR (Near Infrared-Short wave Infrared)-based vegetation indices were more effective in detecting vegetation alterations than NIR-Red-based vegetation indices (Wilson and Sader 2002).

The majority of existing studies to date have used passive optical remote sensing, in which the change or standardized change of different vegetation indices are adopted as damage indicators with little effort to assess their quantitative relationship with forest damage at the pixel level and with little comparative analysis on the performance of these vegetation indices (Hanssen et al. 2021; Lacerda et al. 2021; Landry et al. 2021; Moody et al. 2021). Due to the data volume of pixel-based analysis and continuous Earth observation, studies require continuous time series data with highly configured computer platforms and storage (Gorelick et al. 2017; Kumar and Mutanga 2018; Salcedo-Sanz et al. 2020). For instance, to create a global land cover map for any particular time point, almost 10,000 Landsat scenes or 3 TBs of storage are needed (Giri et al. 2013). High-performance cloud computing platforms have made it possible to store, process, and analyze geographic data at a massive scale on the cloud at a low cost and effectively (Hansen et al. 2013; Giri et al. 2013). In 2010, Google introduced Google Earth Engine (GEE) platform with more than forty years of satellite imagery at no cost (USGS 2014; Dong et al. 2016). Amazon Web Service (AWS) also now provides access to the Landsat data archive, enabling analysis of this dataset on the cloud (Amazon 2015; USGS 2015). Recently NASA (National Aeronautics and Space Administration) launched NASA Earth Exchange Program (NEX), which allows the processing and analysis of NASA Earth observation data (NASA 2021).

With the aid of cloud computing, in this study, we aim to bridge the gap left by earlier research utilizing the land cover change technique and calculate possible hotspots while considering the existence of water bodies and greenness following a catastrophic storm event. Using geospatial computing methods, we estimate the urban vegetation damage and land cover change caused by a significant hurricane along the Gulf Coast. The specific objectives of this study are to estimate land cover changes after a major hurricane landfall on the Gulf Coast, and identify hotspots for rapid post-hurricane urban vegetation assessment.

2. Materials And Methods

2.1. Study area

The Gulf Coast has a history of experiencing hurricanes and tropical storms landfall in the Summer-Fall season. Since 1900, the Gulf Coast has been devastated by 46 hurricanes, and since 1990, the frequency of hurricanes in this area has grown by 70% (NOAA, 2020). Recent years (since 2017) show an early start of hurricane season and NOAA's Climate Prediction Center (CPC) alarms of no respite in terms of a significant decrease in Categories 3, 4 and 5 hurricanes in the Gulf Coast (NOAA, 2021b). Panama City and Panama City Beach are located in the southeastern United States in the area of northwest Florida known as the Panhandle, greatly affected by Hurricane Michael in 2018 (Fig. 2). More than 3 million tourists visit Panama City every year, and this number is likely to increase to more than 5 million by the end of 2050 (Panama City Beach 2022). Around 0.90 million people live in surrounding census county divisions (CCD), and it is estimated to be more than 1.6 million by 2050 (U.S Census Bureau, 2021). Panama City and Panama City Beach are dominated by forestland (21.14%) and woody wetlands (35.54%), which are significantly affected by catastrophic hurricanes. However, urban lands (5.30%) comprise a small portion of the total land use in Panama City and Panama City Beach (MRLC, 2017).

2.2. Image Preprocessing

Figure 3 shows the overall methodology of our study. We used LANDSAT derived multi-spectral data products on the open-source GEE Platform. Considering the track of Hurricane Michael with landfall time (October 10, 2018), we selected Landsat 8 cloud-free satellite images, including vegetation indices on GEE within 90 days prior to the landfall date (Table 1). To find the ideal cloud-free (< 10%) image on the event day, we employed the object-based "CFmask" technique in GEE. "CFmask" is a C programming based function of mask, which is a translation of "Fmask" developed by USGS Earth Resources Observation and Science (EROS) (Zhu and Woodcock 2012; Zhu et al. 2015; Foga et al. 2017). After employing "CFmask", cloud-masked photos were saved in GEE Assets via "Asset Manager" for eventual replication.

Table 1
Description of spatial data requirements for land use change analysis

Data Layer	Source	Scale/Spatial Resolution	Date/Year
Panama City Boundary	Bay County, Florida Website	Scale 1:12880 (meter)	2017
Hurricane Michael (AL142018)	National Hurricane Center (NHC), Florida	Scale 1:12880 (meter)	October 10, 2018; 0735 Central Daylight Time
Landsat 8 Surface Reflectance (SR)	Google earth engine (GEE) data provided by U.S. Geological Survey (USGS)	30	Pre: May 1, 2018 Post: January 28, 2019
National Agriculture Imagery Program (NAIP)	Google earth engine (GEE) data provided by U.S. Department of Agriculture (USDA)	1	2019
Digital Elevation Model (DEM)	Google earth engine (GEE) data provided by NASA/USGS/Jet Propulsion Laboratory-Caltech	30	2000
Enhanced Vegetation Index (EVI)	Google earth engine (GEE) data provided by U.S. Geological Survey (USGS)	30	Pre: May 1, 2018 Post: January 28, 2019
Normalized Difference Water Index (NDWI)	Google earth engine (GEE) data provided by U.S. Geological Survey (USGS)	30	Pre: May 1, 2018 Post: January 28, 2019

2.3. Land cover categories and reference data

Along with the requirements of image processing, land cover analysis also needs reference datasets, land cover classification, indices evaluation, and statistical analysis for pre and post hurricane events. Land cover change detection technique applied and evaluated on GEE platform using Random Forest (RF) classifier algorithm. Random Forest (RF) classifier has been widely used in land cover change studies over the years (Pelletier et al. 2016; Rwanga and Ndambuki 2017; Pimple et al. 2018; Oliphant et al. 2019; Qu et al. 2021). The RF classifier has been effective in the classification accuracy when applied to analyze data with stronger noise (Breiman 2001; Schmidt et al. 2016; Tian et al. 2016). The RF is an ensemble classification approach that creates an ensemble of classification (using multiple decision trees) by employing bootstrap aggregating, or "bagging," where each tree trains on a different subset of the whole training data (Breiman 2001; Waske and Braun 2009).

Classifying heterogeneous land cover from satellite images is a challenging task (Sidhu et al. 2018; Zurqani et al. 2018). Considering the size and scale, we identified four major land covers for Panama City; 1) vegetation, 2) impervious layer, 3) water body, and 4) barren land. For the accuracy assessment of the land cover classification, reference dataset is an important element (Rodriguez-Galiano et al. 2012; Zurqani et al. 2018). We delineated 305 reference points on NAIP images (2019) by visual inspection in the GEE platform randomly using Eq. (1) adopted from (Cochran 1977).

$$n = \frac{(\sum W_i S_i)^2}{\left[S(\hat{O})\right]^2 + (1/N)\sum W_i S_i^2} \approx \left(\frac{\sum W_i S_i}{S(\hat{O})}\right)^2 \quad (1)$$

where N = number of units in the study area, S(O) is the standard error of the estimated overall accuracy that we would like to achieve, W_i is the mapped proportion of the area of class i, and S_i is the standard deviation of stratum i, S_i is the standard deviation of the stratum I, $S_i = \sqrt{(U_i(1-U_i)}$ (Cochran 1977).

A training dataset that consisted of 70% randomly selected observations was created; the remaining 30% of the observations were used in the validation data set (Olofsson et al. 2014). The training dataset was used to improve the supervised classifier algorithm, while the validation dataset was used in the accuracy assessment of the produced land cover classification maps.

2.4. Accuracy assessments and change detection

The purpose of accuracy assessment is to estimate the error and uncertainty of the output classification, to either choose the most appropriate mapping procedure or to inform the interpretation of the output (Olofsson et al. 2014; Lyons et al. 2018). The produced land cover maps were validated using field-verified GPS point data in Panama City and Panama City Beach. One-third (~ 100) of field locations were verified using handheld precision GPS, Google Spreadsheet using mobile hotspots and Google Maps. Finally, a confusion matrix of land cover maps was calculated to evaluate the accuracy of the outputs using producer's accuracy, user's accuracy, and kappa statistics.

Change detection of land cover is the final step to demonstrate change analysis that designates differences between images of the same scene at different times (You et al. 2017; ESRI 2022). Mosaic plot method of GEE was used to represent the gain and loss of the land cover change. The mosaic plot provides a statistical summary of losses and gains over time (Google Earth Engine 2019). Our study used Change Detection Technique in ArcGIS Pro and Image Difference Technique in GEE to see the difference between the two different images taken before the hurricane event and after the hurricane event.

To produce the greenness and wetness of the components for validating land cover change, we used EVI and NDWI for each image scene (before and after the hurricane) using at-sensor reflectance values and stacked them for later classification. We used EVI instead of NDVI because of its additional correction capability for some atmospheric and canopy background noise, and EVI is also more sensitive in areas with dense vegetation (USGS 2016; Vermote et al. 2016). On the other hand, NDWI is used to highlight

open water features in a satellite image, allowing a water body to “stand out” against the soil and vegetation (EOS 2019; Oliphant et al. 2019). We used EVI and NDWI in the GEE platform to process the normalized index values for greenness and wetness in Panama City and Panama City Beach after the hurricane event. GEE JavaScript for this analysis is available in the supplementary file.

2.5. Optimized Hot Spot Analysis (OHS) and Optimized Outlier Analysis (OOA)

We used Optimized Hot Spot Analysis (Getis-Ord Gi*) tool in ArcGIS Pro platform to determine the observed hotspots and coldspots using indices (EVI and NDWI) derived from our input data and Eq. (2). The resultant z-scores and p-values indicate where features with either high or low values cluster spatially. This tool looks at each feature within the context of neighboring features (Getis and Ord 1992; Xiao et al. 2016; Hakim et al. 2021). A feature with a high value is interesting but may not be a statistically significant hotspot. To be a statistically significant hotspot, a feature will have to have a high value and be surrounded by other features with high values as well.

$$G_i^* = \frac{\sum_{j=1}^{n} w_{ij}x_j - \bar{x}\sum_{j=1}^{n} w_{ij}}{S\sqrt{\frac{n\sum_{j=1}^{n} w_{ij}^2 - \left(\sum_{j=1}^{n} w_{ij}\right)^2}{n-1}}} \quad (2)$$

where x_i is the attribute value for feature *j*, w_{ij} is the spatial weight between feature *i* and $_j$, n is equal to the total number of features.

We used optimized outlier analysis to evaluate the characteristics of the input NDWI and EVI values. This analysis interrogates input data to determine settings that will produce optimal cluster and outlier analysis results. The tool calculates a local Moran's I value, a z-score, a pseudo p-value, and a code representing the cluster type for each statistically significant feature. The z-scores and pseudo p-values represent the statistical significance of the computed index values and are measures of statistical significance that tell us whether or not to reject the null hypothesis, pixel by pixel (Anselin 1995; ESRI 2019a). The Local Moran’s I statistic of spatial association is given as:

$$I_i = \frac{x_i - \bar{X}}{S_i^2} \sum_{j=1, j\neq i}^{n} w_{i,j}(x_j - \bar{X}) \quad (3)$$

where x_i is an attribute for feature *i*, X is the mean of the corresponding attribute, $w_{i,j}$ is the spatial weight between feature *i* and *j*, and;

The cluster/outlier type (COType) field in the output table distinguishes between a statistically significant cluster of high values (HH), cluster of low values (LL), outlier in which a high value is surrounded primarily by low values (HL), and outlier in which a low value is surrounded primarily by high values (LH). A high positive z-score (+ + quadrants) for pixels indicates that the surrounding pixels have similar values (either high values or low values) and a low negative z-score (-- quadrants) for pixels indicates a statistically significant spatial data outlier. Statistical significance is set at the 95% confidence level. When no FDR (False Discovery Rate) correction is applied, features with p-values smaller than 0.05 are considered statistically significant (Columbi Public Health 2019; ESRI 2019b). The FDR correction reduces this p-value threshold from 0.05 to a value that better reflects the 95% confidence level given multiple testing. (ESRI 2019c).

3. Results

3.1. Land use change and distribution

Figure 4 shows the significant land cover transition before and after Hurricane Michael in the southwestern part of Panama City Beach. Table 2 shows the land cover transition matrix before and after the hurricane. Over the study period for pre- and post-hurricane, 69.93% of the total study area remained unchanged, while 30.07% changed. The barren land area declined by 20.50% after the hurricane. The abrupt change from barren land to impervious layer and vegetation cover shows how our supervised classification correctly detected this type of land cover transition. Since the post-hurricane image was taken on January 2019, some regeneration was identified in the southwestern part of Panama City Beach. Inland water inundation after the hurricane increased by 19.64%, which infers heavy rainfall and flooding on the shoreline and inland of Panama City and Panama City Beach during the event. The overall accuracies of the supervised images (Table 3) were 81.44% (pre-hurricane) and 80.01% (post-hurricane), respectively. It is likely that classification accuracy was reduced by the variation in the availability of high-resolution imagery from the NAIP that was not always available for the same time period as the Landsat scenes.

After land cover consolidation (Table 4), i.e., vegetation and non-vegetation, intensive rainfall (122 mm ~ 6 hours), and wind speed (252 km/h) on the landfall day (National Weather Service 2018) resulted in vegetation loss of 4.91%. As the hurricane track passed through Panama City Beach, our study found coastal vegetation and woody wetlands loss was about 34.44% of the total vegetation loss (Figures S1 & S2).

Table 2
Land cover transition matrix of Panama City and Panama City Beach. Units are in hectares.

		Post-Michael			
Pre-Michael	*Land Class*	Barren Land	Impervious Layer	Vegetation	Water Body
	Barren Land	0	530.01	701.37	89.73
	Impervious Layer	314.19	0	198.27	35.73
	Vegetation	677.43	440.64	0	58.59
	Water Body	71.46	42.21	42.21	0

Figure 5 illustrates the standard error of the land cover classes before and after the hurricane event. Error bars provide the accuracy of the land cover classification by measuring the pixel as sample variability. Data are more variable for the impervious layer, and our analysis shows standard error for water bodies is negligible before and after the event, even though more areas were inundated by the hurricane induced storm surge.

Table 3
Accuracy assessment of land cover transition after Hurricane Michael.

	Pre-Michael	**Post-Michael**
Training Accuracy	99.23%	99.85%
Validation Accuracy	81.44%	80.01%
Producers Accuracy	78.29%	81.57%
Kappa coefficient	0.69	0.72

Table 4
Vegetation cover change (in hectares) after Hurricane Michael. Percentage in the parenthesis shows the share of total land use of vegetation and non-vegetation.

	Pre-Michael	**Post-Michael**	**Relative Change**
Vegetation	37753 (24.63%)	35987 (23.48%)	-4.91%
Non-vegetation	115543 (75.37%)	117309 (76.52%)	1.51%

3.2. NDWI and EVI change detection

NDWI positive threshold has been increased in the southwestern part of Panama City Beach and northeastern part of Panama City after the hurricane event. While limiting the low reflectance of water characteristics, the near-infrared wavelengths maximize the high reflectivity of terrestrial vegetation and soil components. Water and moisture content (> 0.2) are identified after Hurricane Michael reflects the intensity of heavy rainfall during the event (Fig. 6). The loss of green foliage, which should be directly connected with a fall in EVI and indirectly correlated with a reduction in total chlorophyll and water content at the canopy level, is the most recognizable aspect of sudden canopy alteration that can be detected by optical remote sensing. The hurricane impact identified by EVI than NDWI was consistent with damage severity assessed by the USDA Forest Service, Forest Inventory and Analysis (Clark et al., 2006). The impacted area detected by NDWI was smaller (< 11%) than EVI, while NDWI underestimated the impacted area and did not differentiate the damage level as well as EVI. Based on the analysis, we discovered that, to a certain extent, both NDWI and EVI could identify post-hurricane vegetation damage. Therefore, we further analyzed only the statistical properties of pixel-based NDWI and EVI hotspot analysis.

The Southwestern part of Panama City Beach and the northeastern part of Panama City were identified with more green cover loss than the surrounding inland area. Figures 6 and 7 show mixed characteristics after the hurricane, since the image was taken in January – analysis found some of the canopy and wetland regeneration in the affected area. More water content (> 7.6%) was found in the affected area by the NDWI analysis, which reflects the non-seasonality effect of hurricane season. NDWI seasonality can be found in the supplementary Figure S5 for the years 2014–2018. The histogram distribution (Figures S3 & S4) shows the increment mean shift after the hurricane, reflecting the water intrusion in the study area during the hurricane. However, EVI shows different scenarios than NDWI as the overall mean values (Figure S5 and S6) for EVI increased after the hurricane event. The restoration of the green canopies and green grasslands following the incident was one factor in the increase in EVI values. Histogram of the EVI values (Figure S4) shows the regenration of the green canopies in Panama City and Panama City Beach. Average values of EVI in the previous years during hurricane season (June-October) were 9.31% higher than that of 2018.

3.2. Optimized hotspot and outlier analysis

Using the Getis-Ord Gi* statistic (Eq. 2), optimized hotspot (OHS) analysis evaluated the characteristics of the input feature class (EVI and NDWI) to produce optimal results. OHS automatically aggregated the NDWI and EVI point data by pixel, identified an appropriate scale of analysis for Panama City and Panama City Beach, and corrected for both multiple testing and spatial dependence. When we set the scale of analysis to the pixel level (30x30m), the optimal fixed distance band is based on the average distance to 30 nearest neighbors – 114 to 148 meters depending on the indices value inside our study area boundary.

OHS results are shown in Fig. 8 (NDWI) and Fig. 9 (EVI) according to bin values which identify statistically significant hotspots and coldspots. Valid features and outliers of NDWI and EVI changed after the hurricane because of the indices value transformation. Before the hurricane, the total number of

statistically significant NDWI hotspots (≥ 95% confidence, z ≥ 1.96) covered 61.02% of Panama City and Panama City Beach. Pixels with water bodies were observed to be stable through the time since the last major weather event. Statistically significant hotspots of NDWI increased to 76% after the hurricane as more water inundated the study area. Statistically significant hotspots of EVI increased from 58.78–69.82%, which infers vegetation loss occurred in the southwestern and northeastern parts of Panama City and Panama City Beach respectively. OOA shows hotspots area clustered with 84.01% of the study area, which increased to 91.34% after the hurricane. It indicates more lands are inundated and more and urban vegetation are enriched with the water content by the heavy precipitation and storm surge in the southwestern part of Panama City and Panama City Beach (Figs. 8 and 9). On the other hand, OHS and OOA analysis show vegetation loss due to hurricane, which is represented by the lower number of statistically significant (≥ 95% confidence, z ≥ 1.96) EVI clusters. 65.46% area was clustered, considering the greenness of the vegetation before the hurricane, which decreased to 56.29% after the event (Fig. 10). Figure S7 and S8 illustrated the spatial cluster and outlier of the indices NDWI and EVI before and after the hurricane event.

Our output feature class in ArcGIS Pro created Local Moran's I Index, z score, p-value and cluster/outlier types. Using Eq. (3), we showed the Moran'I cluster and outlier distribution (Figs. 11 & 12). OOA uses spatial lag as a variable to transform z scores which averaged the neighboring values of locations. The transformed z-score values when using a 95% confidence level are confined in -1.96 and + 1.96 standard deviations. Accounting for 66% of the pixels values before the event, our observed p-value was smaller than 0.05, rejecting our null hypothesis because the pattern exhibited could very likely be the result of random spatial processes. Our post-event NDWI scenario observed a similar distribution but with a higher number of point locations. Transformed z values (≥ 95% confidence, z ≥ 1.96) of the outliers for NDWI after the hurricane event decreased to 8.66%, which inferred more similar pixel values in the clustered pattern. Outliers of EVI show relatively static change, increasing to 8.91% from 7.56%, which suggests that more green areas (i.e. small herbs, shrubs, etc.) transformed to barren land or open space.

Figure 13 shows the area of the local sum for each pixel and its neighbors in the affected CCDs (Census County Divisions). This area is then compared proportionally to the sum of all other pixels, leading to a high-high and low-low clustering pattern when significant Z score (≥ 95% confidence, z ≥ 1.96) and vegetation indices are taken into account. Less water content on urban vegetation was found in Panama City than the Panama City Beach because of proximate location near the shoreline. Vegetation cover in Southport and Youngstown was highly affected due to high wind speed (> 250 km/h) as these CCD's are dominated by highly densed coastal woody wetlands. Panama City and Lynn Haven experienced less vegetation damage because of the availability of greater impervious layer. Our analysis found Panama City Beach, Southport and Youngstown CCD as hotspots in terms of high water content in sustained vegetation (NDWI) and overall vegetation condition (EVI) after the Hurricane Micheal.

4. Discussion

Our findings demonstrate the effectiveness of applying optimized hotspot analysis and optimized outlier analysis to identify groups of changes in urban green cover that are connected to water content enrichment. Optimized hotspot analysis and Optimized outlier analysis have the ability to identify spatial patterns in low and high density areas. We demonstrated that location, land use, and vegetation indices, such as NDWI and EVI, can be used to assess how a devastating hurricane will affect built environments and human activities. We discovered various hotspot applications in earth observation, even though optimal hotspot and outlier analysis uses parameters obtained from input data features to conduct the Hot Spot Analysis (Getis-Ord Gi*) tool. For instance, responders employed GIS-based hotspot analysis during Hurricane Harvey (2017) to assist hurricane victims in isolated parts of Texas (Kotak et al. 2018). Hauser et al. (2015) used hotspot technique to assess the wetland degradation pattern after Hurricane Sandy. Van Coppenolle and Temmerman (2020) identified global hotspots for wetland conservation with a global scale GIS hotspot model. Shell et al. (2021) created hotspot maps to characterize the structural diversity of the U.S outer coastal plain mixed forest. Harris et al. (2017) used ArcGIS hotspot analysis to identify the emerging hotspots of forest loss in Brazil.

Our findings from the study and the literatures cited in the study showed hotspot analysis as a good starting point for those interested in understanding where future adverse climate effects i.e. storm surge, sea level rise, drought etc. may occur. However, our study executed an initial data assessment of the input features including data outliers. Since each pixel's neighborhood is defined using pixel-based analysis in order to determine statistical significance, the relative increase in hotspots in our optimized hotspot analysis as time changes makes obvious sense. This research did not account for any changes in the scale of analysis by comparing the pixel sizes of all data layers before and after the event. The pixel's intrinsic value provided the transformation of the changes in land cover brought on by the vegetation indices. The significant changes in hotspot placement under the different neighborhood distances also represent the need for multiscale hotspot analysis that has been identified in the scientific literature to help decision-making at numerous scales across a variety of social challenges (Liu et al. 2017; Guo et al. 2021; Lv et al. 2022).

Water, tree, and wind damage from hurricanes are particularly important in the coastal area with relatively high concentrations of materials and people, whereas wind effects are likely most important in generating tree damage from hurricanes (i.e., defoliation, broken stems, and branches, and uprooted or toppled trees). From the satellite imagery and other ground observations after the hurricane event, changes in water bodies along with the coastal wetlands are evident in the study area. When compared to the long-term impact of the hurricane, impermeable land surface and grasslands exhibit relatively bigger changes. The natural resurfacing of water bodies, slow development of small plants and trees, and regeneration of coastal wetlands all assist in adjusting the shift in land use. Though land cover change is a relatively static process; altercation of natural land use changes due to hurricanes brings about rapid changes. Wind speed is likely to be the most important determinant of tree losses, and numerous factors influence a stand’s resistance to wind loading. Although some factors typically cannot be modified by land use management (e.g., climate, topography, soil conditions), numerous tree management activities

can influence factors that affect a stand's resistance to wind loading. These factors relate to tree species, stand configuration, and silvicultural treatments (Cole et al. 2021).

More coastal communities are vulnerable to the damaging effects of hurricanes as a result of climate change, which has become more apparent in recent years (C2ES 2017; IPCC 2020; Knutson et al. 2020). It is possible that the hotspots we identified could expand geographically and/or increase in intensity under continued climate change. Such expansion or intensification could further complicate hazard mitigation decision-making in hot spot areas, particularly for areas that are not currently considered a hotspot but may become so in the future, including areas in the southeast and pacific northwest. In order to accurately anticipate future climatic events in our study area, it is necessary to go beyond simply characterizing the sites of previous hurricanes and add information on the factors that influence storm activity, such as climate and human activities. Our results can have wide implications on hazard mitigation planning. On the Gulf Coast, hurricanes are a common occurrence, and they are having an increasing impact on progressively larger areas, necessitating greater research (Blake et al. 2005; Rappaport 2014; NOAA 2017). Since there are so few studies that deal with the immediate assessment of hurricane damage on urban vegetation cover, our work may aid professionals and academics in their ongoing research and initiatives. Land use change was prompted by hurricane risk, and our findings offer important information on hazard vulnerability. Although it can be challenging to spot small-scale changes in land use brought on by hurricanes, our research looked for land use transitions and losses of green cover within a short period of time. Findings from our study will assist state policymakers, and this information may also be used at the local jurisdiction level to alert communities of the risk involved in adhering to the Federal Emergency Management Agency's (FEMA) Hazard Mitigation Plan and its recommended procedures (FEMA 2018).

5. Conclusion

It is evident from our research that green cover loss and the presence of water vapor turned the land cover into a different one once a major hurricane hit. Hurricanes can cause significant damage to coastal states, and the current rise in storm frequency is concerning. The findings of our study should be used to help determine where hurricane hazard mitigation techniques should be prioritized and concentrated throughout the Gulf Coast. Although our primary focus is on the effect of hurricanes on the cities on the Gulf Coast, it is possible to use similar methods to characterize other natural disasters in other regions. We analyzed the impact of hurricane in a mid size urban area in the Gulf Coast. Future research could investigate the regional scale (i.e. entire Gulf Coast urban areas) analysis using smaller pixel sizes and finer-scale aggregation patterns, such as those gained from using satellite-based land use changes.

By examining the scale of analysis setting on the ArcGIS Pro platform to characterize the unique land cover type throughout the study area, further research could enhance our techniques. This study worked only on one major hurricane event, more analysis could be done on different intensities of hurricanes and on different cities representing a variety of land use patterns. For the regions that have historically had frequent visits from large hurricanes, a comparison of various intensities is essential. Analyzing the land

use change pattern is important for the Gulf Coast to oversee some land use types, especially wetlands, grasslands, and barren lands. Future research could examine additional, more in-depth land cover transitions besides vegetation in compliance with the NLCD (National Land Cover Database) land use classes.

The statistical analysis used in this study presents a method for evaluating how a natural hazard changed land cover types over time. In the realm of hazard mitigation, this knowledge can play an important role for planners and decision-makers, especially given how climate change is affecting the frequency, intensity, and seasonality of many natural hazards. In essence, climate change is making historical patterns of hazard occurrences less reliable as indicators of future occurrences, which will require hazard mitigation planners to use different techniques for determining probabilities of future occurrence and risk mapping. Planners for risk mitigation should endeavor to include more advanced methods in their risk analyses to represent the complexity of naturally occurring risks influenced by climate. Understanding the spatiotemporal variation in hazard occurrence is one of many things that can help determine where mitigation projects are most needed, give a quantitative check on long-held beliefs about where hazards are most likely to occur, and lay the groundwork for future research to find out why hazards occur where they do and what might be causing the spatiotemporal variation.

Declarations

Conflict of Interest

The authors declare no conflict of interest.

Funding Support

Research reported in this publication was supported by the Gulf Research Program of the National Academies of Sciences, Engineering, and Medicine under award number 200011513. The content is solely the responsibility of the authors and does not necessarily represent the official views of the Gulf Research Program or the National Academies of Sciences, Engineering, and Medicine

Acknowledgments

Authors are thankful to scientists who provided their critical inputs to develop the research and participated in the research discussion for the successful completion of this research.

Authors' Contribution

AA collected and analyzed the data, developed the model, and wrote the first draft of the manuscript. DM supervised the methods and provided technical inputs, PD conceptualized the research, wrote the manuscript, and supervised the overall research. All authors read and reviewed the manuscript.

References

1. Amazon (2015) USGS Landsat - Registry of Open Data on AWS. https://registry.opendata.aws/usgs-landsat/. Accessed 8 Aug 2022
2. Anselin L (1995) Local Indicators of Spatial Association—LISA. Geogr Anal 27:93–115. doi: 10.1111/j.1538-4632.1995.tb00338.x
3. Aosier B, Kaneko M, Takada M (2007) Evaluation of the forest damage by typhoon using remote sensing technique. Int Geosci Remote Sens Symp 3022–3026. doi: 10.1109/IGARSS.2007.4423481
4. Ayala-Silva T, Twumasi YA (2004) Hurricane Georges and vegetation change in Puerto Rico using AVHRR satellite data. Int J Remote Sens 25:1629–1640. doi: 10.1080/01431160310001595037
5. Blake ES, Rappaport EN, Jarrell JD, Landsea CW (2005) The deadliest, costliest, and most intense united states tropical cyclones from 1851 to 2004 (and other frequently requested hurricane facts). Florida
6. Breiman L (2001) Random Forests
7. C2ES (2017) Hurricanes and Climate Change - Center for Climate and Energy SolutionsCenter for Climate and Energy Solutions. https://www.c2es.org/content/hurricanes-and-climate-change/. Accessed 8 Aug 2022
8. Chambers JQ, Fisher JI, Zeng H, et al (2007) Hurricane Katrina's carbon footprint on U.S. Gulf Coast forests. Science (80-) 318:1107. doi: 10.1126/science.1148913
9. Cochran WG (1977) Sampling Techniques, 3rd Edition
10. Cole J, Nowak DJ, Greenfield Jason Cole jasoncole EJ, et al (2021) Potential Hurricane Wind Risk to US Rural and Urban Forests. J For 119:393–406. doi: 10.1093/jofore/fvab018
11. Columbi Public Health (2019) False Discovery Rate | Columbia Public Health. https://www.publichealth.columbia.edu/research/population-health-methods/false-discovery-rate. Accessed 25 Jul 2022
12. Dong J, Xiao X, Menarguez MA, et al (2016) Mapping paddy rice planting area in northeastern Asia with Landsat 8 images, phenology-based algorithm and Google Earth Engine. Remote Sens Environ 185:142–154. doi: 10.1016/J.RSE.2016.02.016
13. EOS (2019) Normalized Difference Water Index: NDWI Formula And Calculations. https://eos.com/make-an-analysis/ndwi/. Accessed 19 Apr 2022
14. ESRI (2022) Change Detection in Amazon Floodplains Using Landsat Time Series
15. ESRI (2019a) How Hot Spot Analysis (Getis-Ord Gi*) works—ArcGIS Pro | Documentation. https://pro.arcgis.com/en/pro-app/2.8/tool-reference/spatial-statistics/h-how-hot-spot-analysis-getis-ord-gi-spatial-stati.htm. Accessed 27 Apr 2022
16. ESRI (2019b) What is a z-score? What is a p-value?—Help | ArcGIS Desktop. https://desktop.arcgis.com/en/arcmap/10.5/tools/spatial-statistics-toolbox/what-is-a-z-score-what-is-a-p-value.htm. Accessed 25 Jul 2022
17. ESRI (2019c) How Cluster and Outlier Analysis (Anselin Local Moran's I) works—ArcGIS Pro | Documentation. https://pro.arcgis.com/en/pro-app/2.8/tool-reference/spatial-statistics/h-how-

cluster-and-outlier-analysis-anselin-local-m.htm. Accessed 18 Jun 2022

18. FEMA (2018) Mitigation Best Practices | FEMA.gov. https://www.fema.gov/emergency-managers/risk/hazard-mitigation-planning/best-practices. Accessed 8 Aug 2022
19. Getis A, Ord JK (1992) The Analysis of Spatial Association by Use of Distance Statistics. Geogr Anal 24:189–206. doi: 10.1111/j.1538-4632.1992.tb00261.x
20. Giri C, Pengra B, Long J, Loveland TR (2013) Next generation of global land cover characterization, mapping, and monitoring. Int J Appl Earth Obs Geoinf 25:30–37. doi: 10.1016/J.JAG.2013.03.005
21. Google Earth Engine (2019) Compositing and Mosaicking | Google Earth Engine | Google Developers. https://developers.google.com/earth-engine/guides/ic_composite_mosaic. Accessed 25 Jul 2022
22. Gorelick N, Hancher M, Dixon M, et al (2017) Google Earth Engine: Planetary-scale geospatial analysis for everyone. Remote Sens Environ 202:18–27. doi: 10.1016/J.RSE.2017.06.031
23. Guo L, Liu R, Men C, et al (2021) Multiscale spatiotemporal characteristics of landscape patterns, hotspots, and influencing factors for soil erosion. Sci Total Environ 779:146474. doi: 10.1016/j.scitotenv.2021.146474
24. Hakim WL, Lee SK, Lee CW (2021) Land Subsidence Monitoring in Semarang, Indonesia Through Optimized Hot Spot Analysis Based on Time-Series Insar Processing. Int Geosci Remote Sens Symp 3789–3792. doi: 10.1109/IGARSS47720.2021.9554374
25. Hansen MC, Potapov P V., Moore R, et al (2013) High-resolution global maps of 21st-century forest cover change. Science (80-) 342:850–853. doi: 10.1126/SCIENCE.1244693/SUPPL_FILE/HANSEN.SM.PDF
26. Hanssen F, Barton DN, Venter ZS, et al (2021) Utilizing LiDAR data to map tree canopy for urban ecosystem extent and condition accounts in Oslo. Ecol Indic 130:108007. doi: 10.1016/j.ecolind.2021.108007
27. Harris NL, Goldman E, Gabris C, et al (2017) Using spatial statistics to identify emerging hot spots of forest loss. Environ Res Lett 12:. doi: 10.1088/1748-9326/aa5a2f
28. Hauser S, Meixler MS, Laba M (2015) Quantification of Impacts and Ecosystem Services Loss in New Jersey Coastal Wetlands Due to Hurricane Sandy Storm Surge. Wetlands 35:1137–1148. doi: 10.1007/S13157-015-0701-Z/FIGURES/6
29. IPCC (2020) AR6 Synthesis Report: Climate Change 2022 — IPCC. https://www.ipcc.ch/report/sixth-assessment-report-cycle/. Accessed 8 Aug 2022
30. Knutson T, Camargo SJ, Chan JCL, et al (2020) Tropical cyclones and climate change assessment part II: Projected response to anthropogenic warming. Bull Am Meteorol Soc 101:E303–E322. doi: 10.1175/BAMS-D-18-0194.1
31. Kotak C, Tomaszewski B, Golen E (2018) al 3-1-1 Calls Hot Spot Analysis during Hurricane Harvey WiPe-Geospatial Technologies and Geographic Information Science for Crisis Management
32. Kumar L, Mutanga O (2018) Google Earth Engine Applications Since Inception: Usage, Trends, and Potential. Remote Sens 2018, Vol 10, Page 1509 10:1509. doi: 10.3390/RS10101509

33. Lacerda LI de A, da Silveira JAR, Santos CAG, et al (2021) Urban forest loss using a GIS-based approach and instruments for integrated urban planning: A case study of João Pessoa, Brazil. J Geogr Sci 31:1529–1553. doi: 10.1007/s11442-021-1910-4
34. Landry SM, Koeser AK, Kane B, et al (2021) Urban forest response to Hurricane Irma: The role of landscape characteristics and sociodemographic context. Urban For Urban Green 61:127093. doi: 10.1016/j.ufug.2021.127093
35. Liu Y, Bi J, Lv J, et al (2017) Spatial multi-scale relationships of ecosystem services: A case study using a geostatistical methodology. Sci Rep 7:1–12. doi: 10.1038/s41598-017-09863-1
36. Lv F, Deng L, Zhang Z, et al (2022) Multiscale analysis of factors affecting food security in China, 1980–2017. Environ Sci Pollut Res 29:6511–6525. doi: 10.1007/s11356-021-16125-1
37. Lyons MB, Keith DA, Phinn SR, et al (2018) A comparison of resampling methods for remote sensing classification and accuracy assessment. Remote Sens Environ 208:145–153. doi: 10.1016/j.rse.2018.02.026
38. Moody R, Geron N, Healy M, et al (2021) Modeling the spatial distribution of the current and future ecosystem services of urban tree planting in Chicopee and Fall River, Massachusetts. Urban For Urban Green 66:127403. doi: 10.1016/j.ufug.2021.127403
39. NASA (2007) Katrina Damage to Gulf Coast Forests. https://earthobservatory.nasa.gov/images/8357/katrina-damage-to-gulf-coast-forests. Accessed 5 Aug 2022
40. NASA (2021) NASA Earth Exchange | NASA. https://www.nasa.gov/nex. Accessed 8 Aug 2022
41. National Weather Service (2018) Hurricane Michael 2018. https://www.weather.gov/tae/HurricaneMichael2018. Accessed 25 Jul 2022
42. NCEI (2022) Billion-Dollar Weather and Climate Disasters | National Centers for Environmental Information (NCEI). https://www.ncei.noaa.gov/access/billions/. Accessed 13 Jul 2022
43. NOAA (2022) NOAA predicts above-normal 2022 Atlantic Hurricane Season | National Oceanic and Atmospheric Administration. https://www.noaa.gov/news-release/noaa-predicts-above-normal-2022-atlantic-hurricane-season. Accessed 12 Jul 2022
44. NOAA (2021a) Hurricane Costs. https://coast.noaa.gov/states/fast-facts/hurricane-costs.html
45. NOAA (2021b) Land Cover Change. https://coast.noaa.gov/states/fast-facts/land-cover-change.html. Accessed 3 Oct 2021
46. NOAA (2018) LAND USE CHANGE WETLANDS AND URBAN DEVELOPMENT. https://www.aoml.noaa.gov/ocd/ocdweb/ESR_GOMIEA/lulc.html. Accessed 21 Sep 2021
47. NOAA (2020) Hurricanes in History. https://www.nhc.noaa.gov/outreach/history/. Accessed 7 Nov 2021
48. NOAA (2005) Hurricane Katrina - August 2005. https://www.weather.gov/mob/katrina. Accessed 21 Sep 2021

49. NOAA (2017) Hurricanes | National Oceanic and Atmospheric Administration. https://www.noaa.gov/education/resource-collections/weather-atmosphere/hurricanes. Accessed 8 Aug 2022
50. Oliphant AJ, Thenkabail PS, Teluguntla P, et al (2019) Mapping cropland extent of Southeast and Northeast Asia using multi-year time-series Landsat 30-m data using a random forest classifier on the Google Earth Engine Cloud. Int J Appl Earth Obs Geoinf 81:110–124. doi: 10.1016/j.jag.2018.11.014
51. Olofsson P, Foody GM, Herold M, et al (2014) Good practices for estimating area and assessing accuracy of land change. Remote Sens Environ 148:42–57. doi: 10.1016/j.rse.2014.02.015
52. Panama City Beach (2022) Area Information | City of Panama City Beach, FL. https://www.pcbfl.gov/about-us/visitors/area-information. Accessed 25 Jul 2022
53. Pelletier C, Valero S, Inglada J, et al (2016) Assessing the robustness of Random Forests to map land cover with high resolution satellite image time series over large areas. Remote Sens Environ 187:156–168. doi: 10.1016/j.rse.2016.10.010
54. Pimple U, Simonetti D, Sitthi A, et al (2018) Google Earth Engine Based Three Decadal Landsat Imagery Analysis for Mapping of Mangrove Forests and Its Surroundings in the Trat Province of Thailand. J Comput Commun 06:247–264. doi: 10.4236/jcc.2018.61025
55. Qu L, Chen Z, Li M, et al (2021) Accuracy Improvements to Pixel-Based and Object-Based LULC Classification with Auxiliary Datasets from Google Earth Engine. Remote Sens 13:453. doi: 10.3390/rs13030453
56. Rappaport EN (2014) Fatalities in the united states from atlantic tropical cyclones: New data and interpretation. Bull Am Meteorol Soc 95:341–346. doi: 10.1175/BAMS-D-12-00074.1
57. Rodriguez-Galiano VF, Ghimire B, Rogan J, et al (2012) An assessment of the effectiveness of a random forest classifier for land-cover classification. ISPRS J Photogramm Remote Sens 67:93–104. doi: 10.1016/J.ISPRSJPRS.2011.11.002
58. Rwanga SS, Ndambuki JM (2017) Accuracy Assessment of Land Use/Land Cover Classification Using Remote Sensing and GIS. Int J Geosci 8:611–622. doi: 10.4236/ijg.2017.84033
59. Salcedo-Sanz S, Ghamisi P, Piles M, et al (2020) Machine learning information fusion in Earth observation: A comprehensive review of methods, applications and data sources. Inf Fusion 63:256–272. doi: 10.1016/j.inffus.2020.07.004
60. Schmidt M, Pringle M, Devadas R, et al (2016) A framework for large-area mapping of past and present cropping activity using seasonal landsat images and time series metrics. Remote Sens 8:. doi: 10.3390/rs8040312
61. Shell AB, Ojha SK, Sharma A (2021) Region-wide characterization of structural diversity of the U.S. Outer Coastal Plain Mixed Forests Province. For Ecol Manage 488:118979. doi: 10.1016/J.FORECO.2021.118979
62. Sidhu N, Pebesma E, Câmara G (2018) Using Google Earth Engine to detect land cover change: Singapore as a use case Using Google Earth Engine to detect land cover change: Singapore as a use.

Eur J Remote Sens 51:486–500. doi: 10.1080/22797254.2018.1451782

63. The Atlantic (2017) Why Does the Gulf Coast Have So Many Natural Disasters? - The Atlantic
64. Tian S, Zhang X, Tian J, Sun Q (2016) Random forest classification of wetland landcovers from multi-sensor data in the arid region of Xinjiang, China. Remote Sens 8:1–14. doi: 10.3390/rs8110954
65. USDA (2020) Forest Service unites around hurricane-damaged forests | US Forest Service. https://www.fs.usda.gov/inside-fs/delivering-mission/sustain/forest-service-unites-around-hurricane-damaged-forests. Accessed 5 Aug 2022
66. USGS (2014) Google Powers Platform for Earth Science Data and Analysis | U.S. Geological Survey. https://www.usgs.gov/landsat-missions/google-powers-platform-earth-science-data-and-analysis. Accessed 8 Aug 2022
67. USGS (2015) Landsat Commercial Cloud Data Access | U.S. Geological Survey. https://www.usgs.gov/landsat-missions/landsat-commercial-cloud-data-access. Accessed 8 Aug 2022
68. USGS (2016) Landsat Enhanced Vegetation Index | U.S. Geological Survey. https://www.usgs.gov/landsat-missions/landsat-enhanced-vegetation-index. Accessed 19 Apr 2022
69. Van Coppenolle R, Temmerman S (2020) Identifying global hotspots where coastal wetland conservation can contribute to nature-based mitigation of coastal flood risks. Glob Planet Change 187:103125. doi: 10.1016/J.GLOPLACHA.2020.103125
70. Vermote E, Justice C, Claverie M, Franch B (2016) Preliminary analysis of the performance of the Landsat 8/OLI land surface reflectance product. Remote Sens Environ 185:46–56. doi: 10.1016/j.rse.2016.04.008
71. Waske B, Braun M (2009) Classifier ensembles for land cover mapping using multitemporal SAR imagery. ISPRS J Photogramm Remote Sens 64:450–457. doi: 10.1016/j.isprsjprs.2009.01.003
72. Wilson EH, Sader SA (2002) Detection of forest harvest type using multiple dates of Landsat TM imagery. Remote Sens Environ 80:385–396. doi: 10.1016/S0034-4257(01)00318-2
73. Xiao Y, Ouyang Z, Xu W, et al (2016) Optimizing hotspot areas for ecological planning and management based on biodiversity and ecosystem services. Chinese Geogr Sci 26:256–269. doi: 10.1007/s11769-016-0803-4
74. You M, Filippi AM, Güneralp I, Güneralp B (2017) What is the direction of land change? A new approach to land-change analysis. Remote Sens 9:1–18. doi: 10.3390/rs9080850
75. Zurqani HA, Post CJ, Mikhailova EA, et al (2018) Geospatial analysis of land use change in the Savannah River Basin using Google Earth Engine. Int J Appl Earth Obs Geoinf 69:175–185. doi: 10.1016/j.jag.2017.12.006
76. Panama City Beach, FL - Detailed climate information and monthly weather forecast | Weather Atlas. https://www.weather-us.com/en/florida-usa/panama-city-beach-climate#temperature. Accessed 23 Sep 2021

Figures

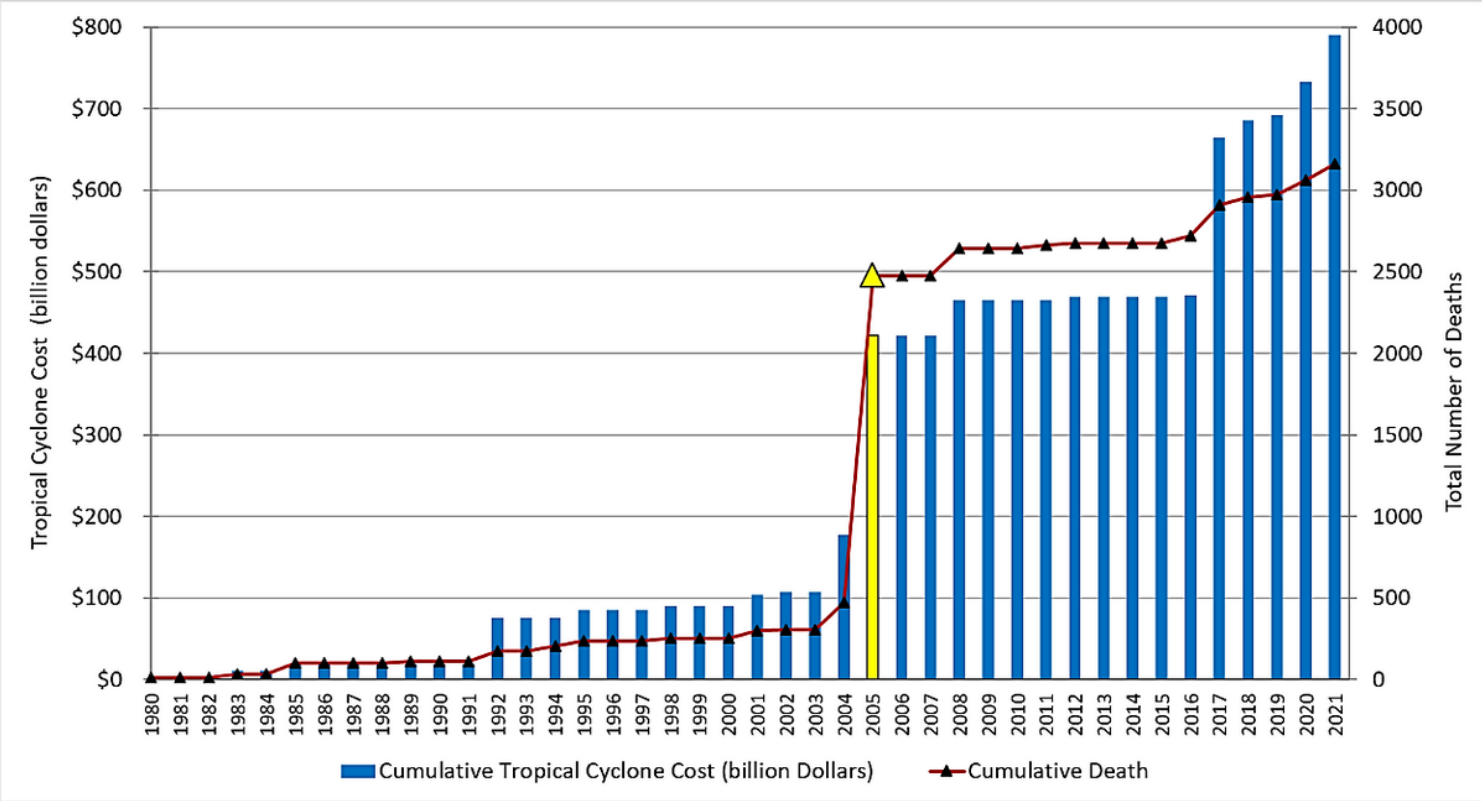

Figure 1

Death and damage costs occurred by tropical cyclones in the Gulf states from 1980 to 2021 (NCEI 2022). Yellow bar in 2005 represents catastrophic Hurricane Katrina.

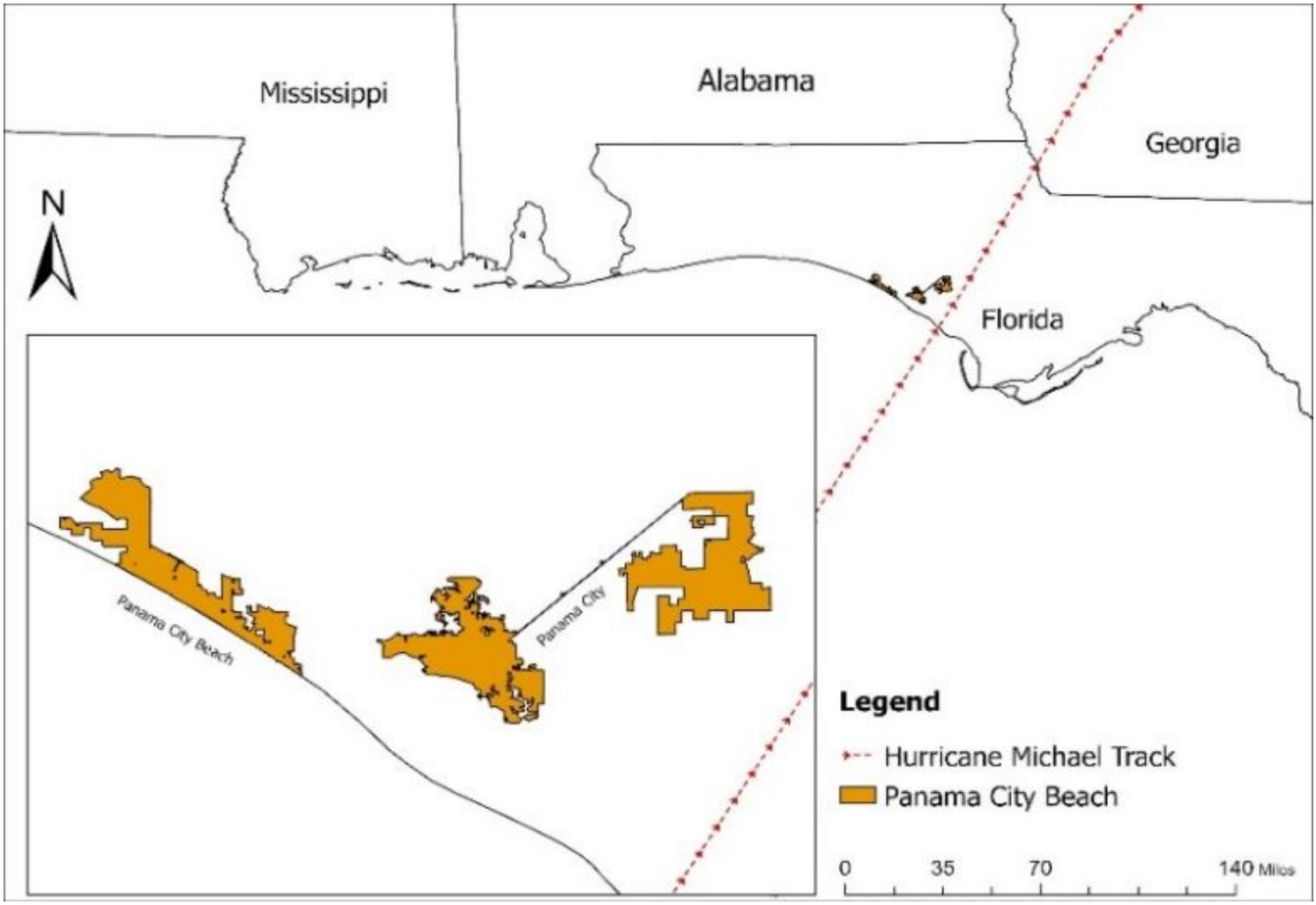

Figure 2

Track of Hurricane Michael (October 10, 2018; 0735 CDT) over Panama City and Panama City Beach, Florida (red dotted line). Key map shows the geographic location of the landfall near Panama City and Panama City Beach (Panama City Beach 2022).

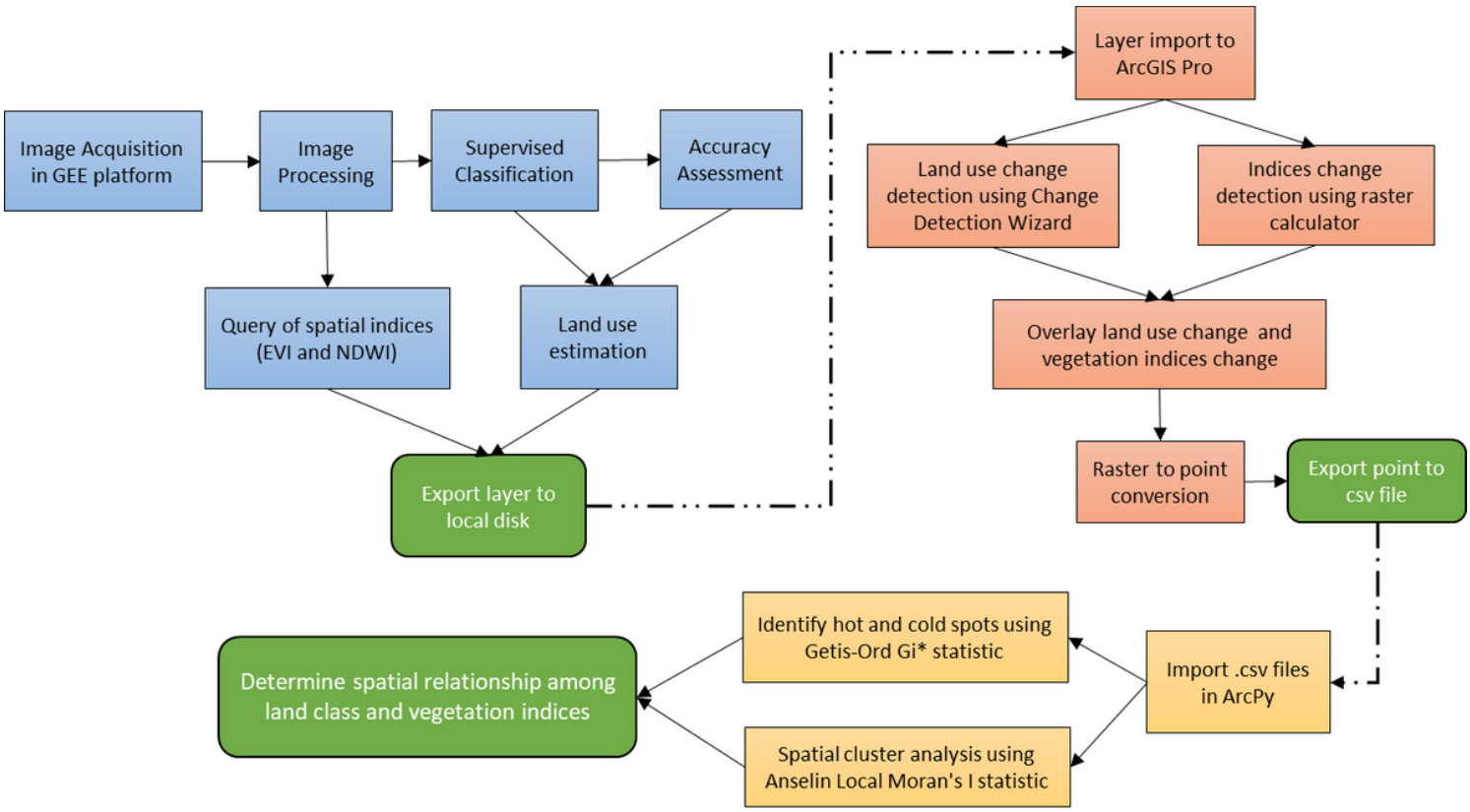

Figure 3

Methodological flowchart of land use change analysis and impact assessment on urban vegetation after a major hurricane.

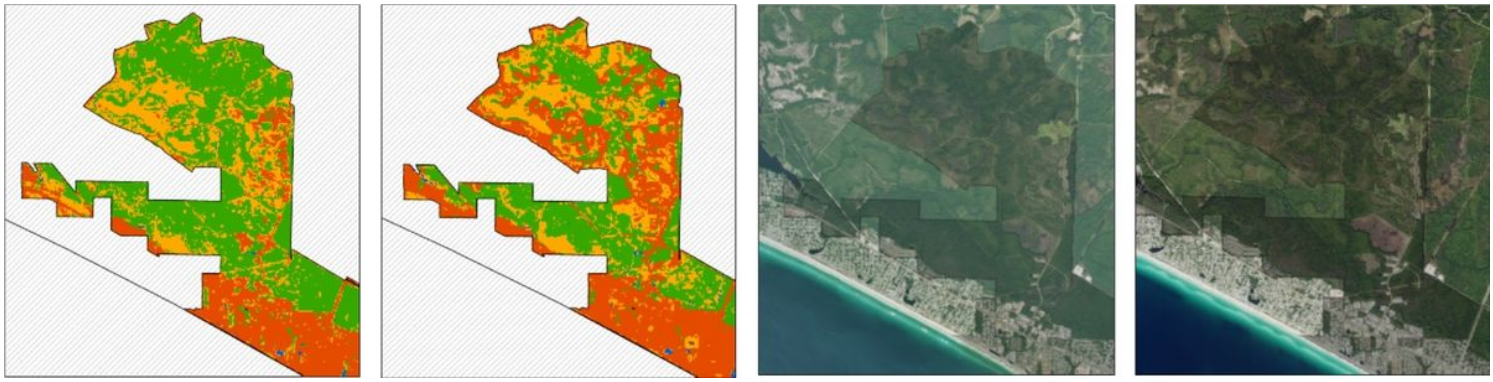

Figure 4

Land cover transition before and after hurricane Michael. (a) supervised land cover on May 1, 2018 (b) supervised land cover on January 1, 2019 (c) NAIP DOQQ, 2015 (d) NAIP DOQQ, 2019

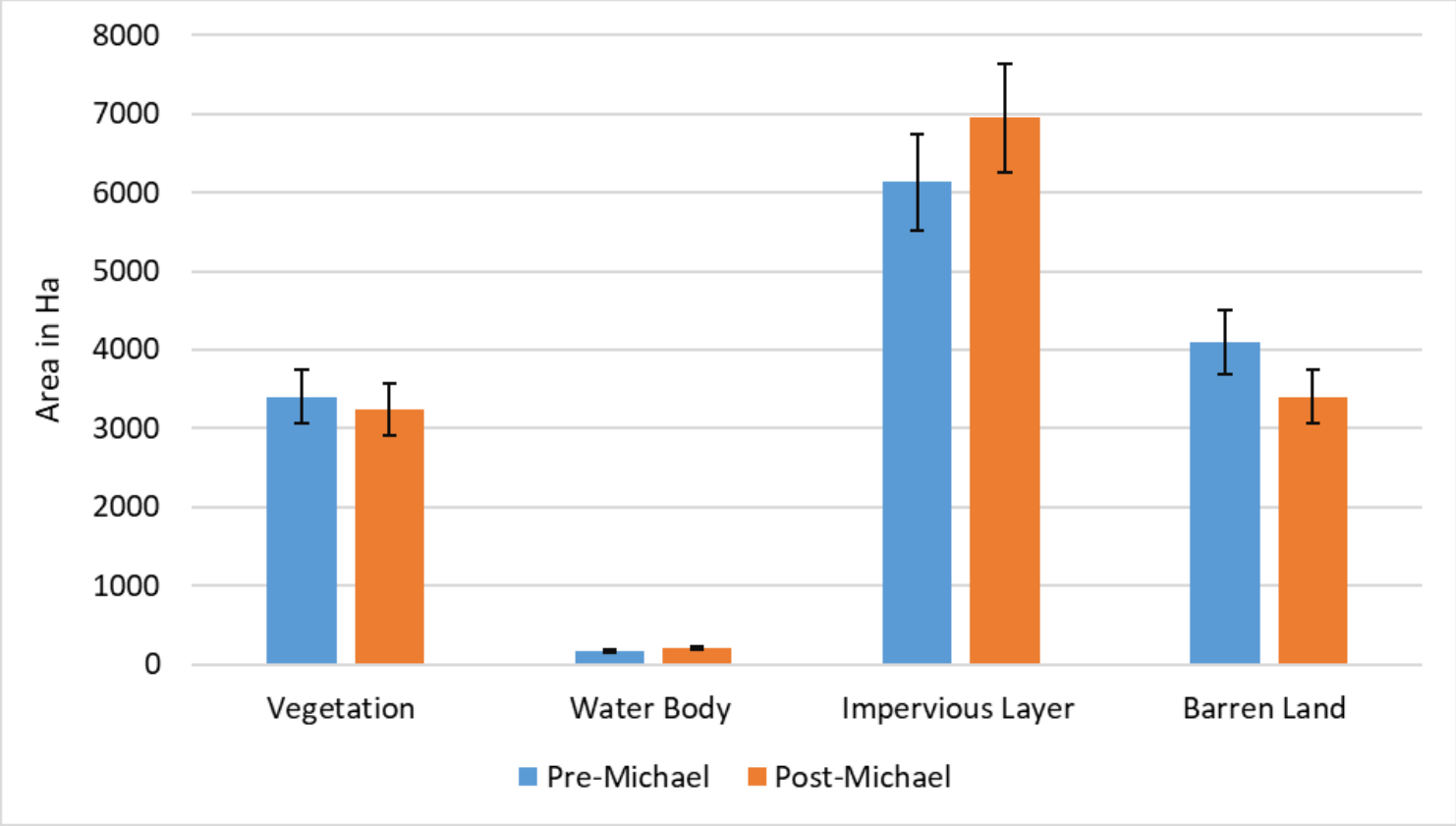

Figure 5

Standard error of land cover classes before and after the hurricane event. Error bars before and after the event overlap, indicating that there is no statistically significant difference between the two time series.

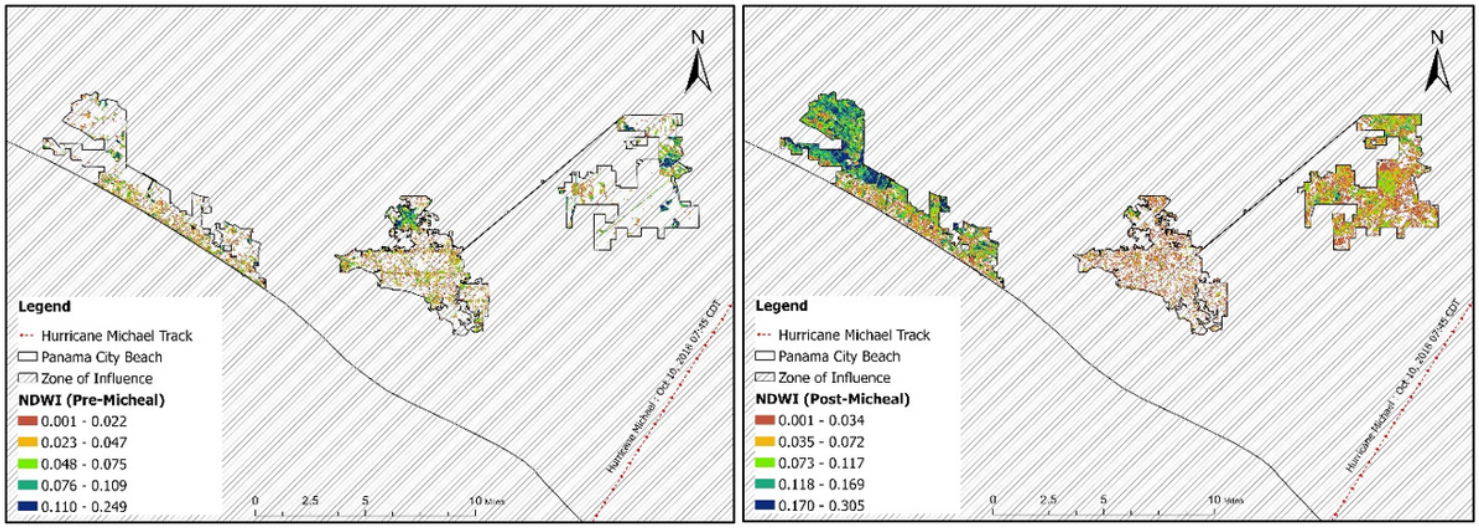

Figure 6

Change of NDWI after Hurricane Michael. Higher values approaching +1 usually appear blue and correspond to either a high-water content or a water surface, while lower values all the way to 0 are the tell-tale signs of drought conditions unless the area of interest is a non-aqueous surface.

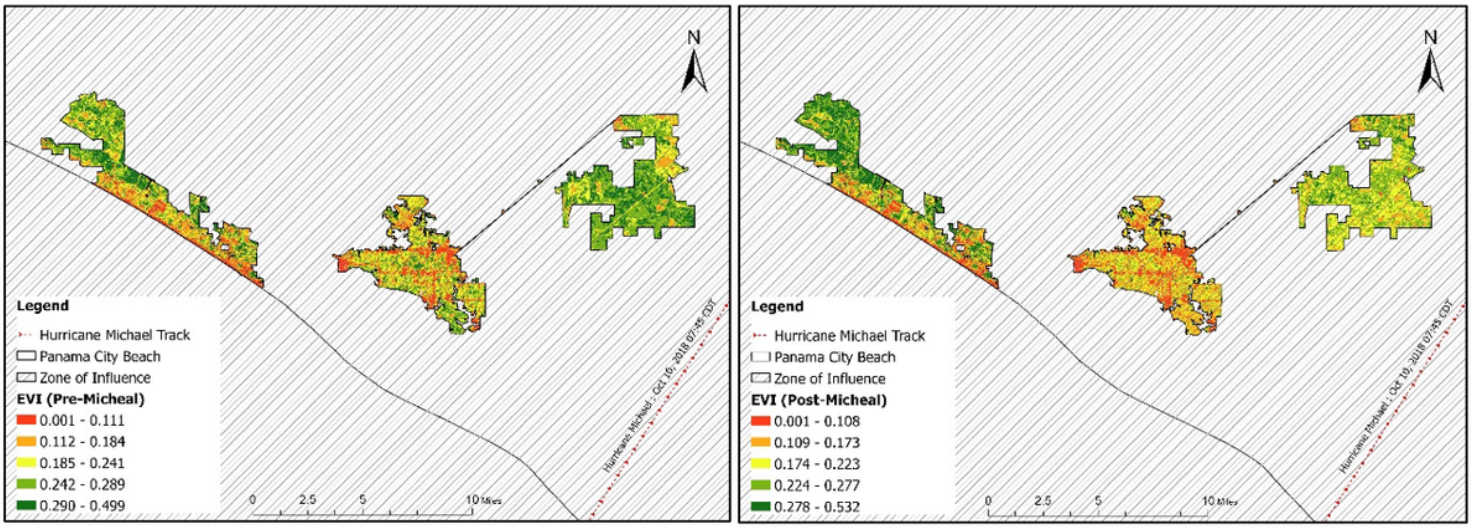

Figure 7

Change of EVI after Hurricane Michael. Negative values are omitted because it corresponds to areas with water surfaces, manmade structures, rocks, clouds, and snow; bare soil usually falls within 0.1- 0.2 range; and plants will always have positive values between 0.2 and 1. Healthy, dense vegetation canopy should be above 0.5, and sparse vegetation will most likely fall within 0.2 to 0.5.

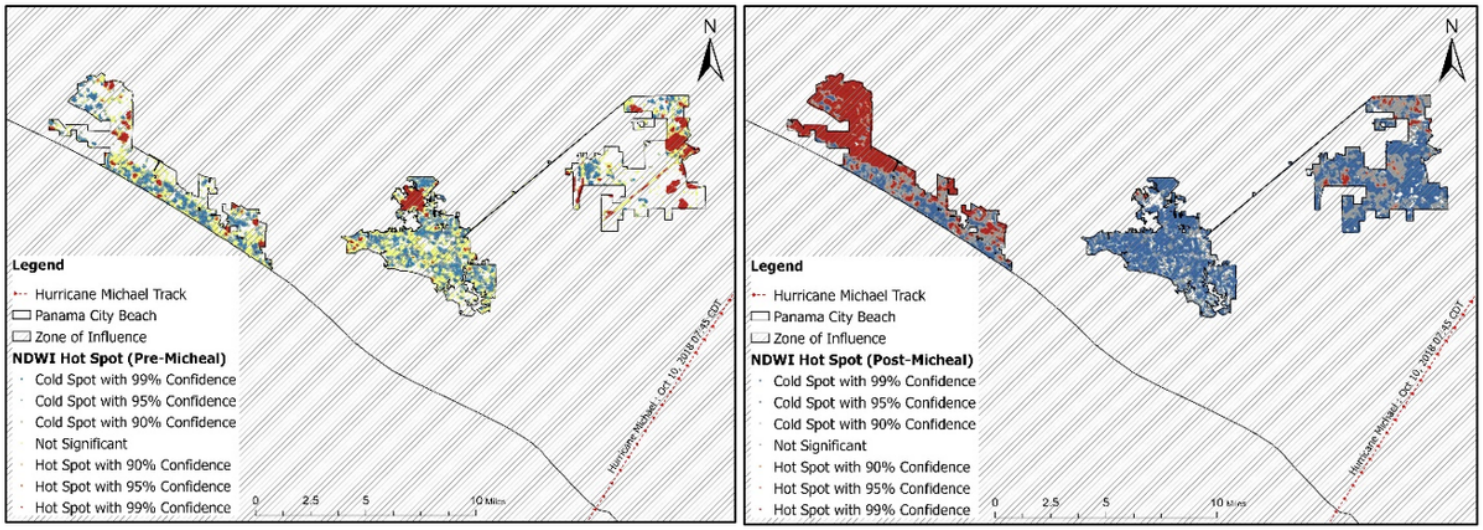

Figure 8

Hotspot and coldspot changes after Hurricane Michael. Red dots are illustrated as hot spots (99% confidence intervals) and blue dots are illustrated as coldspots (99% confidence intervals). Increased NDWI values after the hurricane accumulated in the southwestern part of Panama City Beach.

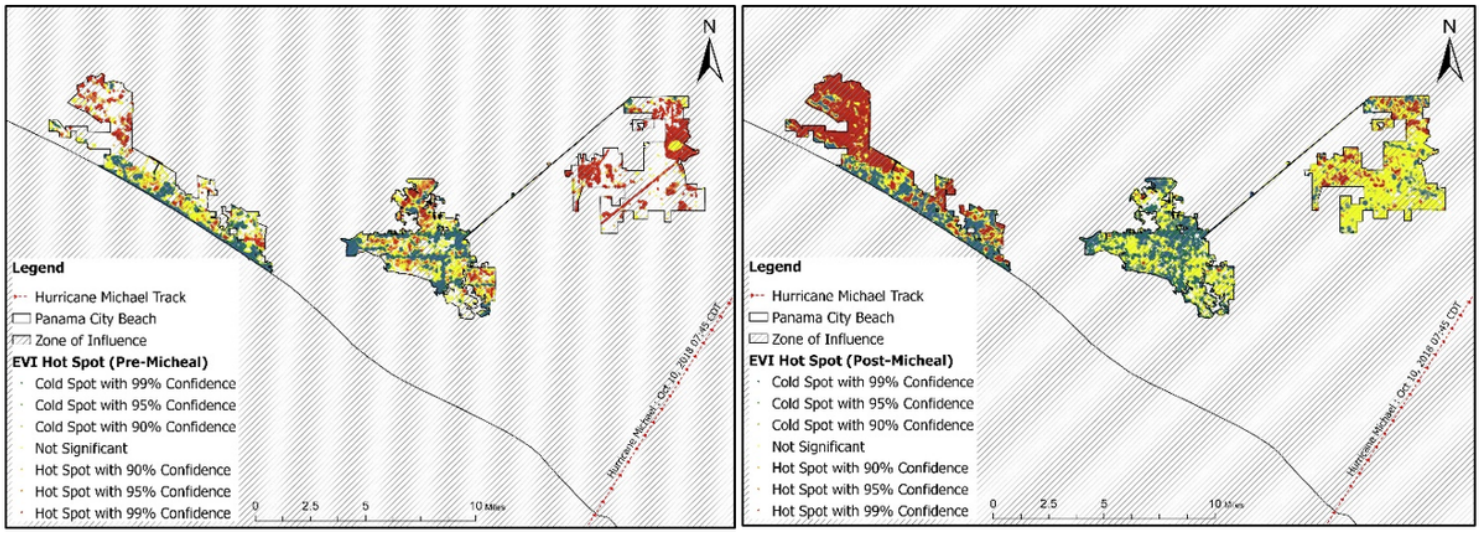

Figure 9

Hotspot and coldspot changes after Hurricane Michael. Red dots are illustrated as hotspots (99% confidence intervals) and yellow dots are illustrated as coldspots (99% confidence intervals). Increased EVI values after the hurricane accumulated in the southwestern part of Panama City Beach.

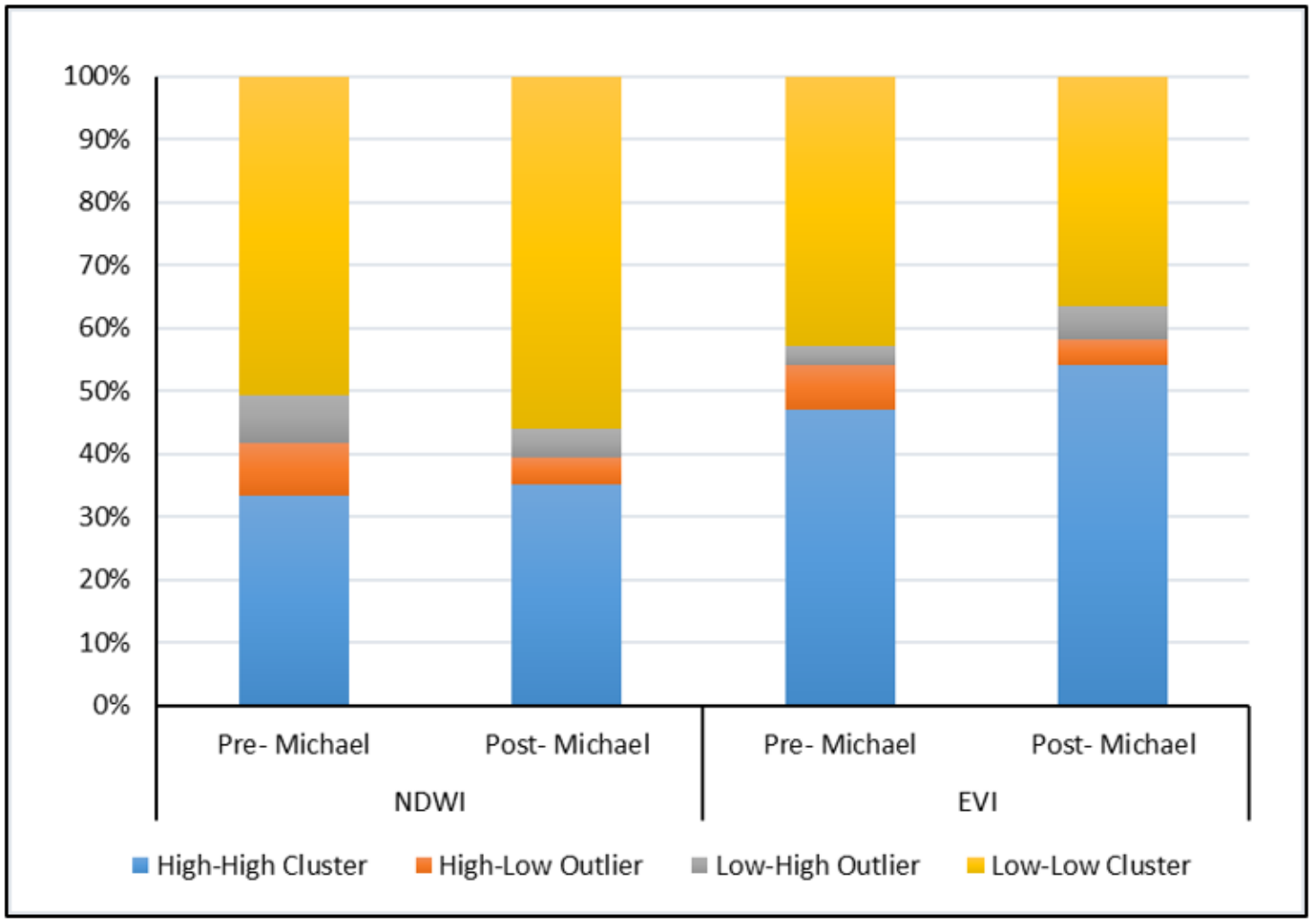

Figure 10

Distribution of statistically significant (≥ 95% confidence, z ≥ 1.96) pixels (cluster and outlier) from OHS and OOA based on the indices before and after Hurricane Michael.

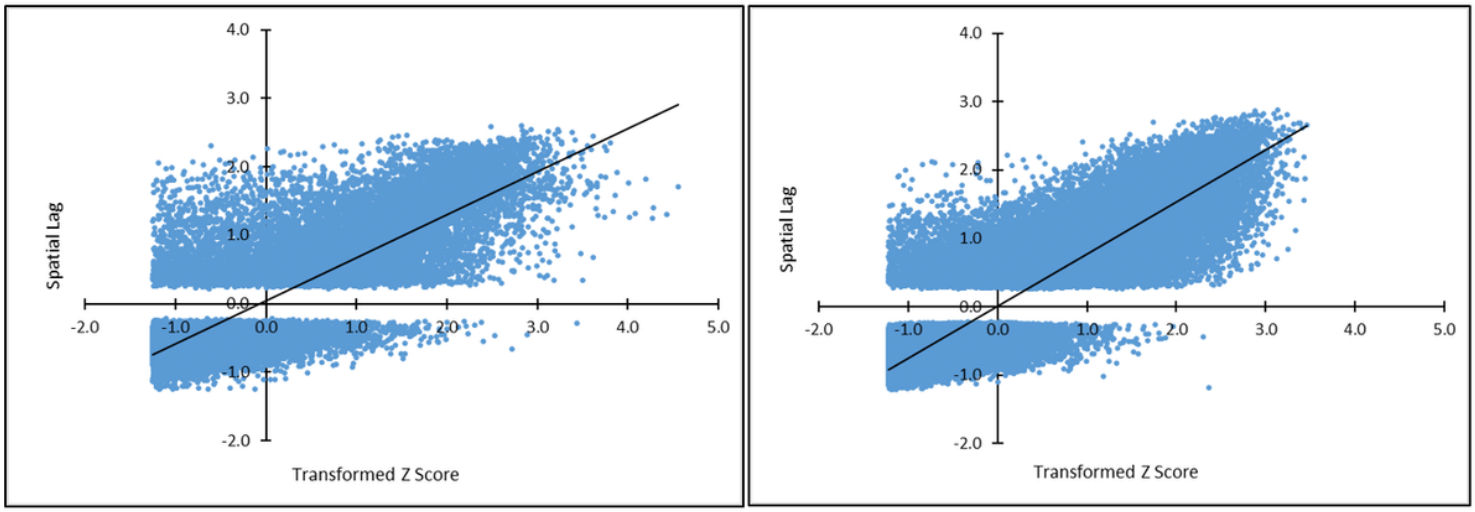

Figure 11

Optimal clusters and outliers based on NDWI before and after Hurricane Michael. Positive-Positive quadrants (++) NDWI values illustrate High-High cluster and Negative-Negative quadrants (–) NDWI values illustrate Low-Low cluster. Positive-Negative (+-) quadrant NDWI values show high-low outliers and Negative-Positive (-+) quadrant NDWI values show low-high outliers.

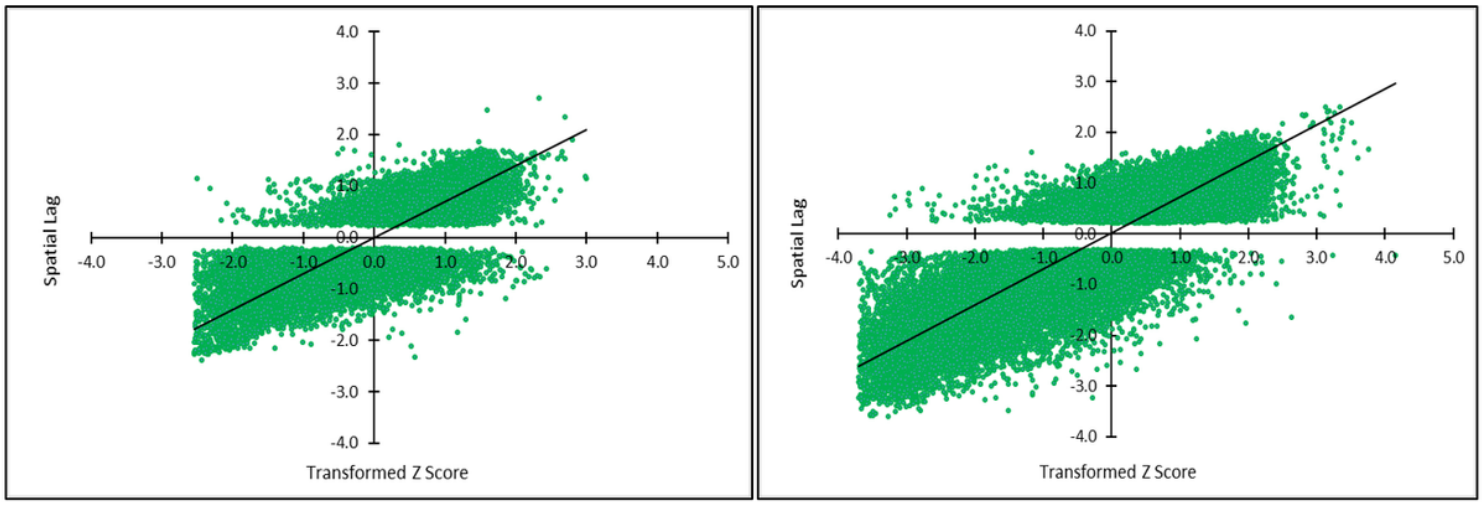

Figure 12

Optimal clusters and outliers based on EVI before and after Hurricane Michael. Positive-Positive quadrants (++) EVI values illustrate High-High cluster and Negative-Negative quadrants (–) EVI values illustrate Low-Low cluster. Positive-Negative (+-) quadrant EVI values show high-low outliers and Negative-Positive (-+) quadrant EVI values show low-high outliers.

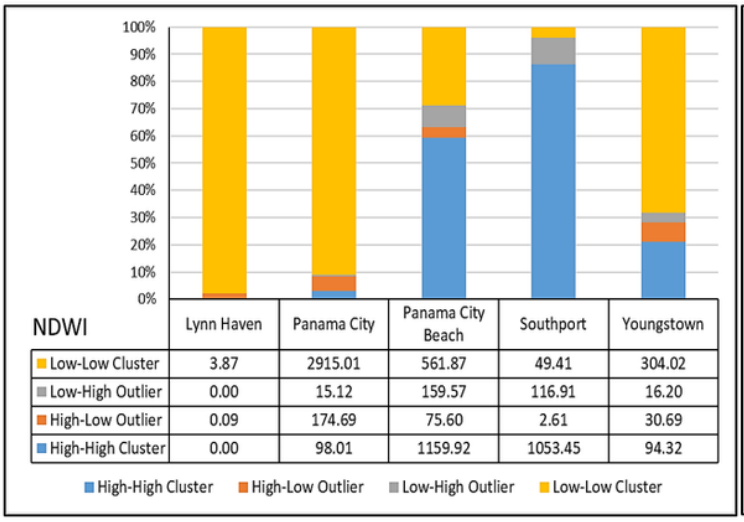

NDWI	Lynn Haven	Panama City	Panama City Beach	Southport	Youngstown
Low-Low Cluster	3.87	2915.01	561.87	49.41	304.02
Low-High Outlier	0.00	15.12	159.57	116.91	16.20
High-Low Outlier	0.09	174.69	75.60	2.61	30.69
High-High Cluster	0.00	98.01	1159.92	1053.45	94.32

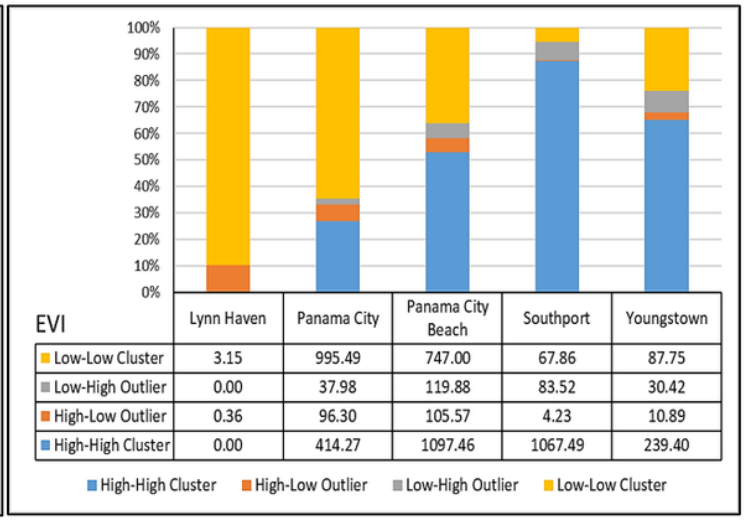

EVI	Lynn Haven	Panama City	Panama City Beach	Southport	Youngstown
Low-Low Cluster	3.15	995.49	747.00	67.86	87.75
Low-High Outlier	0.00	37.98	119.88	83.52	30.42
High-Low Outlier	0.36	96.30	105.57	4.23	10.89
High-High Cluster	0.00	414.27	1097.46	1067.49	239.40

Figure 13

Total area (in hectares) of hotspots in CCD's after the Hurricane Micheal considering NDWI and EVI. Local Moran's I analysis shows High-High clustering pattern observed in Panama City Beach, Southport and Youngstown CCD.

Supplementary Files

This is a list of supplementary files associated with this preprint. Click to download.

- SupplementaryFile.docx